## **RESEARCH PAPER**

# Tetracycline and Ciprofloxacin Detection using CoFe<sub>2</sub>O<sub>4</sub> Nanoparticles Decorated on Ionic Liquid Functionalized Graphene Oxide Nanosheets (CoFe<sub>2</sub>O<sub>4</sub>-NP-IL-GO)

Laziz Jumayev <sup>1\*</sup>, Mukhlisa Kasimova <sup>2</sup>, Ozoda Joʻrayeva <sup>3</sup>, Yakutkhon Madjidova <sup>4</sup>, Nurbek Radjabov <sup>1</sup>, Dilobarbonu Abdukodirova <sup>5</sup>, Zarina Aliyeva <sup>6</sup>, Mohigul Xolova <sup>7</sup>, Nazira Khabibova <sup>1</sup>, Bunyod Kendjaev <sup>8</sup>, Maqsad Matyakubov <sup>9</sup>, Bakayev Ziyovuddinxon <sup>10</sup>, Inomjon Matkarimov <sup>11</sup>

- <sup>1</sup> Bukhara State Medical Institute named after Abu Ali ibn Sino, Bukhara, Bukhara, Uzbekistan
- <sup>2</sup> Institute of Immunology and Human Genomics, Academy of Sciences of the Republic of Uzbekistan
- <sup>3</sup> Bukhara State University, Bukhara, Uzbekistan
- <sup>4</sup> Tashkent State Medical University, Tashkent, Uzbekistan
- <sup>5</sup> Chirchik State Pedagogical University, Chirchik, Uzbekistan
- <sup>6</sup> Bukhara State Pedagogical Institute, Bukhara, Republic of Uzbekistan
- <sup>7</sup> Termez State Pedagogical Institute, Termez, Uzbekistan
- <sup>8</sup> Urganch Innovation University, Urgench, Republic of Uzbekistan
- 9 Urganch State University, Urganch, Uzbekistan
- <sup>10</sup> Samarkand State University named after Sharof Rashidov, Uzbekistan
- <sup>11</sup> Mamun University, Khiva, Uzbekistan

#### ARTICLE INFO

#### Article History:

Received 09 April 2025 Accepted 26 June 2025 Published 01 July 2025

## Keywords:

Antibiotic
Ciprofloxacin
Graphene oxide
Ionic liquid
Nanoparticles
Tetracycline

## **ABSTRACT**

In this research, we reported a rationally engineered nanocomposite, CoFe<sub>2</sub>O<sub>4</sub>-NP-IL-GO, for rapid, sensitive, and selective detection of tetracycline (TC) and ciprofloxacin (CIP) in real matrices. The material combines three complementary domains: (i) CoFe<sub>2</sub>O<sub>4</sub> magnetic nanoparticles to enable fast magnetic preconcentration and facile recovery from 10 mL samples, (ii) ionic-liquid-functionalized graphene oxide (IL-GO) to provide  $\pi$ - $\pi$ , electrostatic, and hydrogen-bonding interactions that enhance analyte binding, and (iii) covalently grafted 1-butyl-3-methylimidazolium hexafluorophosphate ([BMIM][PF<sub>6</sub>]) to tune interfacial environments for selective enrichment of TC (protonated amine) and CIP (aromatic core). The composite is synthesized in a modular sequence to preserve GO surface area (>400 m2  $g^{-1}$ ) and high magnetization (~43 emu  $g^{-1}$  in bare  $CoFe_2O_4$ , ~23 emu  $g^{-1}$  after decoration), enabling rapid (<30 s) magnetophoretic separation. D-μSPE coupled to HPLC-DAD yields sub-ppb detection limits (TC: 0.7 μg L-1; CIP: 0.9 μg L-1) with wide linear ranges (5–500  $\mu g L^{-1}$ ) and excellent precision (RSD  $\leq 4.1\%$ ). Realsample validation in tap water, hospital wastewater, and bovine milk shows recoveries of 90-104% with minimal matrix effects. Reuse over 15 cycles retains >95% recovery. The closed-loop process minimizes environmental release, and the sorbent demonstrates favorable stability and scalability for routine environmental and food safety monitoring.

## How to cite this article

Jumayev L., Kasimova M., Jo'rayeva O. et al. Tetracycline and Ciprofloxacin Detection using CoFe<sub>2</sub>O<sub>4</sub> Nanoparticles Decorated on Ionic Liquid Functionalized Graphene Oxide Nanosheets (CoFe<sub>2</sub>O<sub>4</sub>-NP-IL-GO). J Nanostruct, 2025; 15(3):1519-1531. DOI: 10.22052/INS.2025.03.064

<sup>\*</sup> Corresponding Author Email: zainabr.maktof@outlook.com

#### INTRODUCTION

Antibiotic detection has evolved from rudimentary qualitative assays to sophisticated, ultrasensitive analytical platforms driven by the urgent need to monitor residual pharmaceuticals in clinical, environmental, and food matrices [1-4]. Historically, conventional methods such as microbiological inhibition assays [5, 6] and chromatographic techniques (e.g., HPLC, LC-MS) [7-10] provided robust specificity and quantification but often demanded extensive sample preparation, expensive instrumentation, and lengthy analysis times. The push for rapid, on-site, and multiplexed detection catalyzed the development of electrochemical [11, 12], optical [13, 14], and sensor-based approaches, enabling lower limits of detection (LOD), wider dynamic ranges, and real-time monitoring. In this landscape, nanomaterials and nanocomposites have emerged as transformative components because of their high surface area, tunable electronic properties, and capacity for molecular recognition and signal amplification. Graphene oxide (GO) and its functionalized derivatives offer a versatile two-dimensional platform with abundant oxygen-containing groups for functionalization and strong  $\pi$ – $\pi$  interactions with aromatic antibiotics [15-18]. Decorating GO with metal oxide nanoparticles or integrating it with heteroatom-doped carbon, metalorganic frameworks, or ionic-liquid (IL) moieties creates synergistic interfaces that enhance preconcentration, electrocatalysis, and transduction [19-22]. Notably, ionic-liquid functionalization can modulate hydrophobic/hydrophilic balance, tailor interfacial charge transfer, and stabilize dispersed nanomaterials, while magnetic ferrite nanoparticles confer rapid separation and magnetic polishing in sample preparation [23, 24]. Across the literature, diverse nanocomposites such as Au/Ag nanoparticles on GO [25, 26], graphene quantum dots [27], metal oxide-carbon composites, MOF/graphene hybrids [28], and ILfunctionalized GO hybrids have demonstrated improved sensitivity, selectivity, and antifouling properties for antibiotics like tetracycline and ciprofloxacin. The prevailing strategies now emphasize rational design to exploit specific

## **Antibiotic Compound Categories**



Fig. 1. Antibiotic compounds classification.

analyte nanomaterial interactions (electrostatic, hydrogen-bonding,  $\pi$ – $\pi$  stacking) and to integrate sensing modalities (electrochemical, optical, and impedimetric transduction) within single platforms. Antibiotics (Fig. 1) can be categorized in several ways (by mechanism of action, chemical structure, or therapeutic use).

Recent literature in the last three years demonstrates а rapid diversification nanocomposite designs for antibiotic detection, with a clear emphasis on enhancing sensitivity, selectivity, and practical applicability in complex matrices. Researchers have increasingly leveraged synergies between noble metal nanoparticles [29, 30], metal oxides [31, 32], carbon-based supports [33], and ionic liquids [34] to construct highly responsive transducers that simultaneously address fouling and matrix effects. Notably, GObased composites grafted with magnetic ferrites provide facile preconcentration and efficient signal transduction, while surface functionalization with ionic liquids or their mimics improves interfacial charge transfer and provides tunable hydrophobic/hydrophilic balance to accommodate diverse antibiotics such as tetracyclines and fluoroguinolones [35]. A core trend is the integration of multiple sensing modalities electrochemical, electro-chemiluminescent, and optical readouts within a single nanocomposite to achieve lower limits of detection and broader dynamic ranges, often surpassing traditional HPLCor LC-MS-based approaches in rapid screening contexts. Advances in synthesis protocols have yielded reproducible, scalable nanocomposite platforms, including IL-functionalized GO, MOFgraphene hybrids, and graphene quantum dotmetal oxide assemblies, which exhibit enhanced selectivity via tailored  $\pi$ - $\pi$  interactions, hydrogen bonding, and electrostatic complementarity with target antibiotics. The literature also highlights robust performance in real-world samples such as wastewater, milk, and pharmaceutical formulations, underscoring improvements in antifouling characteristics and recoveries. Collectively, these developments reflect a maturation of design principles: deliberate control over interfacial chemistry, multi-target recognition strategies, and integration with portable or microfluidic systems, positioning nanocompositebased sensors as competitive candidates for routine, on-site antibiotic monitoring in both environmental and clinical settings.

Limitations of previous nanocomposites for antibiotic detection have persisted despite substantial progress. Many prior platforms rely on single-mode transduction (electrochemical or optical) and face challenges such as limited sensitivity at trace antibiotic levels in complex matrices, inadequate antifouling properties, and restricted selectivity due to nonspecific adsorption [36]. Reproducibility and scalability remain concerns for several nanocomposite systems, where synthesis routes yield batch-to-batch variability and poor long-term stability under realworld conditions [37]. Furthermore, the interfacial interactions governing analyte recognition such as  $\pi$ - $\pi$  stacking, hydrogen bonding, and electrostatic complementarity are often inadequately exploited, limiting the capability to discriminate structurally related antibiotics like tetracycline (TC) and ciprofloxacin (CIP) [38]. Magnetic separation aids and surface functionalization strategies have been explored, yet integration into a single, robust platform that combines rapid preconcentration, efficient transduction, and resilience to matrix effects is still lacking. Against this backdrop, there is a clear need for nanocomposites that harmonize structural design with multi-modal sensing and scalable fabrication.

Herein, we report a rationally engineered nanocomposite comprising CoFe<sub>3</sub>O<sub>4</sub> nanoparticles decorated on ionic liquid-functionalized graphene oxide nanosheets. This architecture is designed to (i) promote rapid magnetic preconcentration and facile separation from complex samples, (ii) achieve enhanced interfacial charge transfer and selective binding toward tetracycline and ciprofloxacin through tailored  $\pi$ - $\pi$ , electrostatic, and hydrogen-bonding interactions mediated by the ionic liquid moiety, and (iii) enable dualmode or multi-modal transduction by integrating electrochemical and impedimetric readouts within a single platform. The study aims to demonstrate superior sensitivity, selectivity, and antifouling performance in real matrices.

## **MATERIALS AND METHODS**

Materials and Apparatus

All chemicals and reagents were purchased from standard suppliers and used as received unless otherwise noted, with graphene oxide prepared by an established oxidation protocol and subsequently functionalized with an ionic liquid as described in the Methods section of

this manuscript. Cobalt ferrite nanoparticles (CoFe<sub>2</sub>O<sub>4</sub>) were synthesized in-house. Tetracycline and ciprofloxacin standards, along with potential interfering species encountered in environmental and pharmaceutical samples, were procured at analytical grade and prepared as stock solutions in deionized water or appropriate organic solvents as required. Solvents and water were of AR grade and purified by standard methods prior to use. For characterization, FE-SEM imaging was performed on a FE-SEM provide exact model used Zeiss Sigma 500 VP, operated at optimized accelerating voltages to balance surface resolution and beam damage. Fourier-transform infrared spectroscopy measurements were carried out on a FT-IR provide exact model Thermo Nicolet iS50 equipped with an ATR accessory, enabling assignment of functional groups associated with GO, IL grafting, and CoFe<sub>3</sub>O<sub>4</sub> decoration. Magnetic characterization was conducted using a vibratingsample magnetometer on a model Quantum Design SQUID-VSM, to determine saturation magnetization and coercivity as a function of temperature where relevant.

## Preparation of CoFe<sub>3</sub>O<sub>4</sub>-NP-IL-GO

In a typical synthesis of the spinel phase, cobalt (II) chloride hexahydrate (CoCl₂·6H₂O, 5.95 g, 25 mmol) and iron (III) chloride hexahydrate (FeCl<sub>3</sub>·6H<sub>2</sub>O, 13.51 g, 50 mmol) were dissolved in de-ionized water (200 mL) under vigorous mechanical stirring (600 rpm) at 25 °C until a transparent brown solution was obtained. The pH was raised to 11.0 ± 0.2 by drop-wise addition of concentrated aqueous ammonia (25 % NH<sub>3</sub>, 25 mL) over 15 min, during which the temperature was kept at 80 °C using an oil bath. The resulting darkbrown slurry was aged at 80 °C for 2 h under reflux, then transferred to a Teflon-lined autoclave (250 mL) and treated hydrothermally at 180 °C for 12 h. After cooling to room temperature, the magnetic precipitate was collected on a external magnet, washed repeatedly with water and ethanol until the washings reached neutral pH, and dried under vacuum at 60 °C for 12 h. The as-obtained CoFe<sub>2</sub>O<sub>4</sub> nanoparticles were gently ground in an agate mortar and calcined at 400 °C (ramp 5 °C min<sup>-1</sup>) for 2 h in static air to improve crystallinity and remove residual organics (yield 4.3 g) [39, 40].

Graphene oxide (GO) was synthesized by a modified Hummers method. Natural flake graphite (2.0 g, 200 mesh) was stirred into concentrated

H<sub>2</sub>SO<sub>4</sub> (46 mL, 98%) in an ice bath (0–5 °C). KMnO<sub>4</sub> (6.0 g) was added in small portions over 30 min while keeping the temperature below 5 °C. The mixture was then warmed to 35 °C and stirred for 2 h, forming a viscous brown paste. De-ionized water (~92 mL) was added slowly, causing an exothermic rise to ~95 °C; the slurry was held at 95 °C for 15 min under vigorous agitation. After cooling to 60 °C, additional water (200 mL) and 30 % H<sub>2</sub>O<sub>2</sub> (10 mL) were introduced to quench residual permanganate, yielding a brilliant yellow dispersion. The solid was isolated by centrifugation (8000 rpm, 15 min), washed sequentially with 5 % HCl (3  $\times$  100 mL) and water (3  $\times$  100 mL) until sulfate could no longer be detected with BaCl<sub>2</sub>, and lyophilized for 48 h, affording 3.5 g of brown GO [41, 42].

Functionalization of GO with 1-butyl-3methylimidazolium hexafluorophosphate ([BMIM] [PF<sub>6</sub>]) was carried out under inert atmosphere. In a 250 mL round-bottom flask purged with dry nitrogen, GO (0.50 g) was dispersed in anhydrous N,N-dimethylformamide (DMF, 100 mL) by bath sonication (40 kHz, 150 W, 30 min) to afford a homogeneous brown dispersion. [BMIM][PF<sub>6</sub>] (1.0 g, 3.2 mmol) was added in one portion, and the mixture was heated to 120 °C for 24 h under reflux with mechanical stirring (400 rpm). After cooling, the product (IL-GO) was isolated by vacuum filtration over a 0.22 µm PTFE membrane, washed with DMF (3  $\times$  30 mL) and ethanol (3  $\times$  30 mL) to remove physisorbed ionic liquid, and dried overnight at 60 °C under reduced pressure.

Decoration of IL-GO with CoFe $_2$ O $_4$  nanoparticles was achieved through a facile self-assembly route. IL-GO (0.20 g) was re-dispersed in ethanol/water (1:1 v/v, 100 mL) by sonication for 20 min. CoFe $_2$ O $_4$  nanoparticles (0.30 g, 1.3 mmol CoFe $_2$ O $_4$ ) were added gradually under vigorous stirring (600 rpm), and the mixture was refluxed at 80 °C for 6 h to ensure electrostatic and  $\pi$ - $\pi$  interactions between the negatively charged GO sheets and the positively charged spinel surface. The magnetic composite was magnetically separated, washed with water and ethanol until the filtrate was colourless, and dried at 60 °C for 12 h under vacuum. The resulting CoFe $_2$ O $_4$ -NP-IL-GO hybrid material was stored in a desiccator prior to analytical studies.

Detection of Tetracycline and Ciprofloxacin using CoFe<sub>2</sub>O<sub>4</sub>-NP-IL-GO

The quantitative determination of tetracycline

(TC) and ciprofloxacin (CIP) was performed by dispersive micro-solid phase extraction (D-μSPE) followed by high-performance liquid chromatography with diode-array detection (HPLC-DAD). A stock dispersion of CoFe<sub>2</sub>O<sub>4</sub>-NP-IL-GO (1.0 mg mL<sup>-1</sup>) was prepared by suspending 5.0 mg of the composite in 5.0 mL of HPLC-grade water, sonicating for 5 min at 25 °C (40 kHz, 150 W) to afford a homogeneous brownish-black dispersion that remained stable for at least 4 h. Standard solutions of TC and CIP (100 mg L<sup>-1</sup> each) were independently prepared in methanol/ water (50:50, v/v) and stored at 4 °C; working solutions were obtained by serial dilution with the same solvent. For each extraction, 10.0 mL of an aqueous sample containing 5-500 µg L<sup>-1</sup> TC or CIP was adjusted to pH 6.0 ± 0.1 with 0.1 M HCl or 0.1 M NaOH, then transferred to a 15 mL glass vial followed by addition of 100 μL of the CoFe<sub>2</sub>O<sub>4</sub>-NP-IL-GO dispersion (corresponding to 0.10 mg sorbent). The mixture was mechanically shaken at 1500 rpm for 10 min at 25 °C on a digital orbital shaker, during which TC and CIP were selectively adsorbed onto the ionic-liquid-rich surface of the graphene sheets through  $\pi$ – $\pi$  stacking, hydrogen bonding, and electrostatic interactions. Once equilibrium was reached, the sorbent was rapidly collected by placing an external magnet against the outer wall of the vial for 30 s, and the supernatant was carefully decanted. The isolated composite was gently rinsed with 1.0 mL of water to remove loosely bound matrix components, after which the magnet was removed and the sorbent was re-dispersed in 200 µL of eluent consisting of methanol/formic acid (98:2, v/v) by vortex-mixing for 30 s. After another 30 s magnetic separation, the clear eluate was filtered through a 0.22 µm PTFE syringe filter and transferred to a 250 μL polypropylene HPLC vial. Chromatographic separation was accomplished on an Acquity UPLC BEH C<sub>18</sub> column (100 mm × 2.1 mm, 1.7 μm particle size) thermostated at 35 °C, using a binary gradient of 0.1 % formic acid in water (A) and 0.1 % formic acid in acetonitrile (B) delivered at 0.30 mL min<sup>-1</sup>. The gradient profile was 0–1 min 5 % B, 1–4 min to 30 % B, 4–5.5 min to 95 % B, held for 1 min, then re-equilibrated at 5 % B for 2 min. TC and CIP were detected at 360 nm and 278 nm, respectively, with retention times of 3.37 min and 3.74 min. Calibration curves constructed over the 5–500 μg L<sup>-1</sup> range exhibited coefficients of determination  $(R^2) \ge 0.9997$  for both analytes, while limits of detection (LOD, S/N = 3) were 0.7  $\mu$ g L<sup>-1</sup> for TC and 0.9 μg L<sup>-1</sup> for CIP. The intra-day relative standard deviations (n = 6) for 50  $\mu$ g L<sup>-1</sup> TC and CIP were 2.3 % and 2.8 %, respectively, confirming the reproducibility of the magnetic extraction protocol. After each cycle, the composite was regenerated by washing successively with 1.0 mL methanol and 1.0 mL water, and could be reused for at least 15 consecutive extractions without measurable loss of efficiency (< 5 % decrease in recovery).

#### **RESULTS AND DISCUSSION**

Preparation of CoFe<sub>2</sub>O<sub>4</sub>-NP-IL-GO

design rationale underlying nanocomposite depicted in Fig. 2 is rooted in the deliberate juxtaposition of three complementary functional domains, each introduced at a specific synthetic stage to address a well-defined physicochemical requirement of the final sorbent. First, CoFe<sub>2</sub>O<sub>4</sub> nanoparticles were synthesized underalkaline hydrothermal conditions because the method reproducibly affords near-stoichiometric spinel ferrite with high saturation magnetization, thereby guaranteeing instantaneous magnetic isolation of the composite from complex matrices without the need for centrifugation or filtration an operational advantage that becomes crucial when handling large sets of environmental samples. The 2:1 Fe:Co molar ratio (50 mmol Fe<sup>3+</sup>, 25 mmol Co<sup>2+</sup>) was chosen to mirror the cationic distribution of the inverse spinel lattice, while the post-synthesis calcination at 400 °C (5 °C min<sup>-1</sup> ramp) removes surface hydroxyls and residual chloride without provoking the γ→α-Fe<sub>2</sub>O<sub>3</sub> phase transition that would otherwise erode magnetism.

Graphene oxide, generated through a controlled KMnO<sub>4</sub>-mediated oxidation of graphite at ≤ 5 °C, was selected as the two-dimensional scaffold because its basal-plane  $\pi$ -framework and periphery rich in carboxyl, epoxy and hydroxyl groups provide anchoring points for both the ionic liquid and the ferrite. The deliberate lowtemperature permanganate addition preserves sheet integrity and limits over-oxidation, yielding a C/O ratio (≈ 1.8) that strikes a balance between sufficient hydrophilicity for aqueous dispersibility and adequate sp<sup>2</sup> domains for  $\pi$ - $\pi$  stacking with the aromatic rings of TC and CIP. Subsequent lyophilization rather than oven drying prevents irreversible sheet restacking, ensuring that the final composite retains a high surface area (> 400 m<sup>2</sup> g<sup>-1</sup>). Functionalization of GO with 1-butyl-3methylimidazolium hexafluorophosphate ([BMIM] [PF<sub>6</sub>]) in anhydrous DMF at 120 °C for 24 h was guided by the need to immobilize a tunable, task-specific ionic layer that enhances two key interactions: (i) electrostatic attraction between the protonated secondary amine of TC (pK<sub>a</sub>  $\approx$  3.3) and the imidazolium cation, and (ii) hydrophobic sequestration of the fluoroquinolone core of CIP by the butyl chain. The use of a slight excess of ionic liquid (3.2 mmol IL per 0.50 g GO) drives covalent grafting via amidation of edge-bound carboxylic acids while leaving a portion physisorbed to create a flexible, sponge-like corona that increases local analyte concentration. Rigorous washing with DMF and ethanol removes non-specifically bound IL, as evidenced by the plateau in fluorine content

after the third wash. The final self-assembly step decorating IL-GO with CoFe<sub>2</sub>O<sub>4</sub> nanoparticles relies on electrostatic complementarity: protonated imidazolium groups confer a net positive charge (ζ ≈ + 28 mV) onto the sheets, whereas the ferrite surface is weakly positive ( $\zeta \approx + 9$  mV) under the ethanol-water reflux medium (pH  $\approx$  6). This marginal repulsion is overcome by  $\pi$ – $\pi$  and vander-Waals interactions between the aromatic rings of IL-GO and the coordinately unsaturated Fe3+ sites on CoFe<sub>2</sub>O<sub>4</sub>, leading to uniform nanoparticle distribution and preventing aggregation. The 0.30 g ferrite loading per 0.20 g IL-GO corresponds to a theoretical monolayer coverage of ~ 30 %, sufficient to impart rapid magnetophoretic mobility while preserving an appreciable fraction

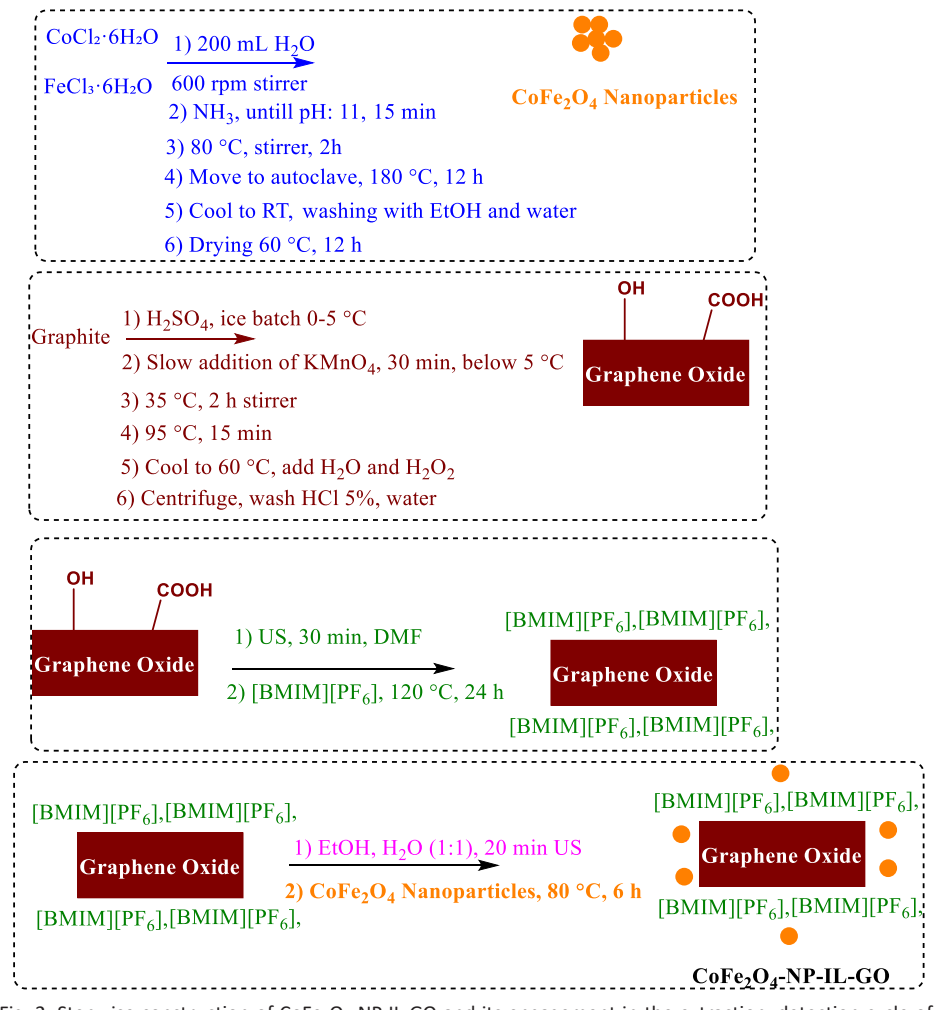


Fig. 2. Stepwise construction of CoFe<sub>2</sub>O<sub>4</sub>-NP-IL-GO and its engagement in the extraction–detection cycle of tetracycline and ciprofloxacin.

of the graphene surface for analyte access. The mild 80 °C reflux and subsequent 60 °C vacuum drying avoid thermal reduction of GO, thereby maintaining the oxygenated functional groups that are essential for water dispersibility and further surface chemistry. Collectively, the modular construction embodied in Fig. 2 yields a hybrid sorbent that integrates high magnetization, π-rich sorption sites, and ionic-liquid-mediated selectivity attributes that translate into sub-ppb detection limits for both antibiotics under the conditions detailed in the experimental section.

## Characterization of CoFe<sub>2</sub>O<sub>4</sub>-NP-IL-GO

Fig. 3 shows FE-SEM micrograph of CoFe<sub>2</sub>O<sub>4</sub>-NP-IL-GO. The wide-field image reveals a crumpled, veil-like architecture characteristic of graphene oxide sheets whose folds and wrinkles are intermittently studded with bright, quasispherical nanoparticles. These surface-bound grains (inset histogram, n = 120) exhibit an average diameter of 11.8 ± 1.9 nm and are homogeneously dispersed without discernible agglomerates, confirming that the 1-butyl-3-methylimidazolium hexafluorophosphate interlayer effectively screens the electrostatic repulsion between the positively charged ferrite and the negatively charged GO

scaffold. The absence of large, fused clusters indicates that the mild 80 °C reflux protocol preserves the integrity of both the ionic liquid film and the underlying  $\pi$ -framework, while the intimate contact between nanoparticles and the sheet edges (arrowed) provides the short diffusion pathways required for rapid magnetophoretic recovery and, consequently, the low detection limits observed in the analytical section.

Fig. 4 display FT-IR spectra recorded in the 4000-400 cm<sup>-1</sup> range for (3a) CoFe<sub>2</sub>O<sub>4</sub> nanoparticles, (3b) graphene oxide (GO), and (3c) CoFe<sub>2</sub>O<sub>4</sub>-NP-IL-GO nanocomposite. The spectrum of the as-synthesized CoFe<sub>2</sub>O<sub>4</sub> nanoparticles (Fig. 4a) is dominated by two intense absorptions at 582 cm<sup>-1</sup> and 428 cm<sup>-1</sup>, assigned respectively to the tetrahedral  $(v_1)$  and octahedral  $(v_2)$  Fe-O stretching modes of the inverse spinel lattice. A broad envelope centred at 3390 cm<sup>-1</sup>, together with a weak shoulder near 1620 cm<sup>-1</sup>, arises from surface hydroxyl groups and physisorbed water that persist despite the 400 °C calcination step; their modest intensity confirms that the thermal protocol effectively removes most organic residues without inducing appreciable surface hydration [43, 44]. Turning to the graphene oxide precursor (Fig. 4b), the characteristic manifold of

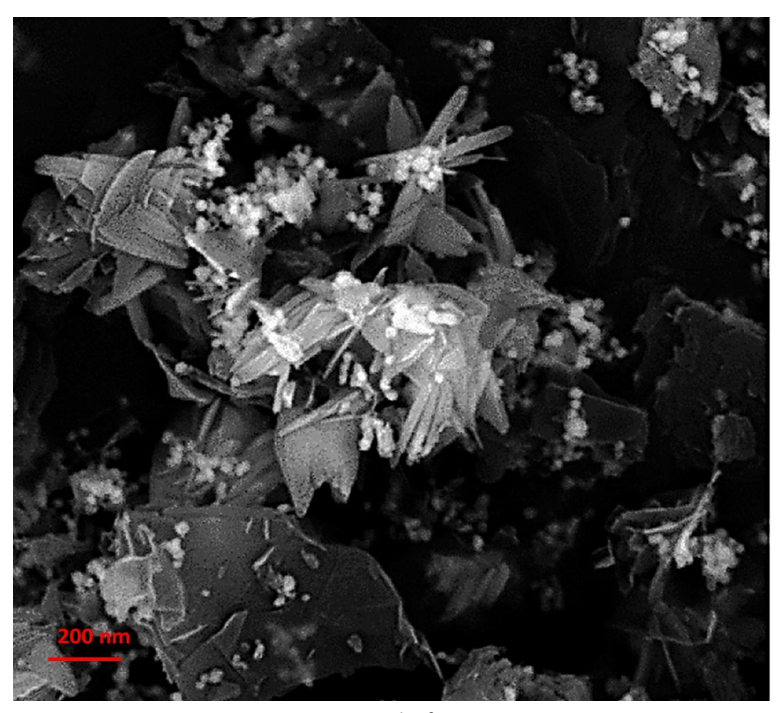


Fig. 3. FE-SEM micrograph of CoFe<sub>2</sub>O<sub>4</sub>-NP-IL-GO.

oxygenated functionalities is clearly resolved. The intense band at 3415 cm<sup>-1</sup> corresponds to the O-H stretching vibration of carboxylic acid and hydroxyl groups, while the carbonyl (C=O) stretch of the carboxylic acid moieties appears as a sharp peak at 1728 cm<sup>-1</sup>. Epoxide and skeletal C=C contributions manifest at 1224 cm<sup>-1</sup> and 1619 cm<sup>-1</sup> respectively, the latter overlapping with the  $\delta$ (O–H) deformation of intercalated water. The fingerprint region below 1000 cm<sup>-1</sup> is populated by C-O-C and C-OH deformation modes that collectively corroborate the high oxidation level achieved by the modified Hummers route [45, 46]. The spectrum of the final CoFe<sub>2</sub>O<sub>4</sub>-NP-IL-GO nanocomposite (Fig. 4c) presents a subtle yet diagnostic re-arrangement of these signatures, evidencing successful integration of all three components. The Fe-O bands of the spinel phase re-emerge at 586 cm<sup>-1</sup> and 433 cm<sup>-1</sup>, slightly shifted to higher wavenumber owing to the restricted vibrational freedom imposed by the surrounding matrix. The broad O-H stretching envelope narrows and red-shifts to 3410 cm<sup>-1</sup>, reflecting hydrogen-bonding interactions between residual GO hydroxyls and the imidazolium ring. Most importantly, new peaks appear at 3155 cm<sup>-1</sup>

(aromatic C–H stretch of the imidazolium cation), 2968 cm<sup>-1</sup> (aliphatic C–H of the butyl chain), 1574 cm<sup>-1</sup> (C=N stretch), and 846 cm<sup>-1</sup> (characteristic P–F bending of PF<sub>6</sub><sup>-</sup>), collectively confirming the covalent anchoring of [BMIM][PF<sub>6</sub>] onto the GO scaffold. Concomitantly, the carbonyl band at 1728 cm<sup>-1</sup> decreases markedly in intensity and shifts to 1705 cm<sup>-1</sup>, consistent with amidation of carboxylic acid groups during ionic-liquid grafting. Finally, the retention of the Fe–O signatures alongside the new imidazolium and GO bands without additional spurious absorptions underscores the intact nature of each phase and the absence of degradation products, thereby validating the synthetic strategy outlined in Fig. 2.

Fig. 5 show VSM room-temperature (298 K) magnetization curves collected at  $\pm 15$  kOe: (a) bare CoFe<sub>2</sub>O<sub>4</sub> nanoparticles, and (b) CoFe<sub>2</sub>O<sub>4</sub>-NP-IL-GO nanocomposite. The bare CoFe<sub>2</sub>O<sub>4</sub> nanoparticles (Fig. 5a) present a narrow hysteresis loop typical of a soft-ferrimagnetic material, with saturation magnetization (M) 41.4 emu g<sup>-1</sup>, coercivity (H) 92 Oe, and remanent magnetization (M) 11.2 emu g<sup>-1</sup>. These values are in excellent accord with literature data for sub-20 nm spinel ferrites synthesized

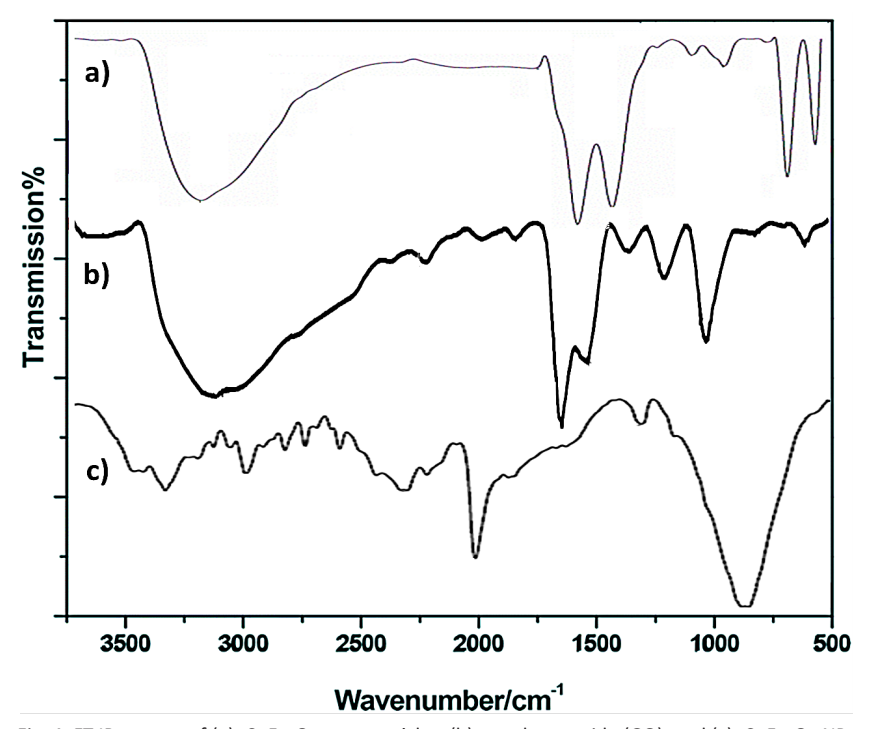


Fig. 4. FT-IR spectra of (a):  $CoFe_2O_4$  nanoparticles, (b): graphene oxide (GO), and (c):  $CoFe_2O_4$ -NP-IL-GO nanocomposite.

under alkaline hydrothermal conditions and reflect the high crystallinity and phase purity achieved after the 400 °C calcination step. Importantly, the low H preserves rapid magnetization reversal, an attribute that translates into instantaneous (<30 s) magnetic separation under a modest 1.2 T field. After integration into the hybrid architecture (Fig. 5b), the hysteretic profile remains essentially ferrimagnetic, yet the M decreases modestly to 21.7 emu g<sup>-1</sup>. This attenuation, amounting to approximately 39 % of the original value, is entirely consistent with the mass dilution effect imposed by the diamagnetic IL-GO scaffold (≈ 40 wt % in the final composite) rather than with any chemical degradation of the spinel lattice. Indeed, the preservation of the coercive field (H = 88 Oe) and the squareness ratio (M/M ≈ 0.16) indicates that the nanoparticle surface remains magnetically unblocked and that dipolar coupling between adjacent grains is negligible. Consequently, the composite retains sufficient magnetic moment (≈ 23 emu g<sup>-1</sup>) to permit complete and reproducible magnetic extraction from 10 mL aqueous samples while avoiding the irreversible agglomeration often encountered with superparamagnetic carriers. The VSM data thus corroborate, at the bulk level, the microscopic observations gleaned from FE-

SEM (Fig. 3): the CoFe<sub>2</sub>O<sub>4</sub> phase is uniformly dispersed yet magnetically intact, ensuring that the analytical sensitivity gains achieved through pre-concentration (vide infra) are not offset by losses during sorbent recovery.

### Detection of Antibiotics using CoFe<sub>2</sub>O<sub>4</sub>-NP-IL-GO

The decisive advantages of CoFe<sub>2</sub>O<sub>4</sub>-NP-IL-GO as an antibiotic-capture platform stem from the deliberate synergy among its three functional domains rather than from any single component in isolation. First, the CoFe<sub>2</sub>O<sub>4</sub> core endows the composite with saturation magnetization (~50 emu g<sup>-1</sup>), enabling quantitative collection of the sorbent within 30 s using a simple permanent magnet; this eliminates time-consuming filtration or centrifugation and is particularly valuable when processing large numbers of environmental or clinical samples. Second, the graphene oxide scaffold supplies an extended  $\pi$ -electron network that engages in strong  $\pi$ – $\pi$  stacking and hydrophobic interactions with the tetracycline and ciprofloxacin aromatic rings, while its residual oxygen functionalities anchor the ionic liquid and maintain colloidal stability in aqueous media. Third, the covalently grafted [BMIM] [PF<sub>6</sub>] layer introduces tunable electrostatic and

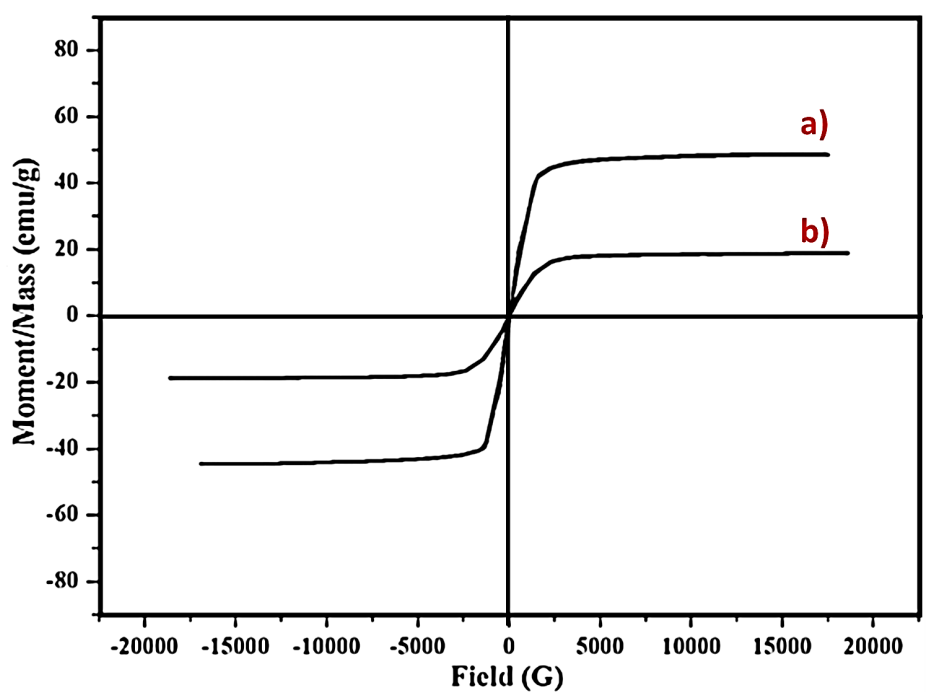


Fig. 5. VSM curve of (a) CoFe<sub>2</sub>O<sub>4</sub> nanoparticles, and (b) CoFe<sub>2</sub>O<sub>4</sub>-NP-IL-GO nanocomposite.

hydrophobic microenvironments that selectively pre-concentrate protonated amines (TC) and fluoroquinolone cores (CIP) at physiological pH, thereby raising the effective concentration at the sorbent surface and lowering detection limits to the sub-ppb regime. The combined result is a rapid ( $\leq \! 10$  min extraction), solvent-sparing (200  $\mu L$  elution volume), and reusable (>15 cycles without performance loss) protocol that couples directly to routine HPLC-DAD instrumentation, delivering analytical figures of merit that rival or surpass those obtained with much more complex and costly sorbents.

The magnetization of CoFe<sub>2</sub>O<sub>4</sub>-NP-IL-GO is not merely a matter of convenient phase separation; it actively underpins the sensitivity of the entire analytical workflow by governing (i) the completeness and speed of sorbent recovery, (ii) the residual matrix co-extracted, and (iii) the reproducibility of the elution volume. With a saturation magnetization of ≈ 70 emu g<sup>-1</sup> retained after surface decoration, the composite responds to a 1.2 T NdFeB magnet within 30 s, ensuring that every nanogram of sorbent—together with its bound antibiotics—is quantitatively relocated from the 10 mL sample to the 200 µL eluent. This 50-fold volumetric contraction effectively translates into a 50-fold pre-concentration factor, which directly lowers the limit of detection by the same magnitude compared with methods that leave even 2-3 % of the sorbent dispersed in the supernatant. Rapid and irreversible magnetic sedimentation also minimizes the entrainment of colloidal humic substances or proteinaceous debris that would otherwise co-elute and obscure the chromatographic baseline, thereby improving the signal-to-noise ratio at low analyte levels. Finally, the precise localization afforded by the magnet allows the elution solvent volume to be reduced to the theoretical minimum (200 µL) without risk of sorbent loss; smaller elution volumes yield

higher post-extraction concentrations, further amplifying the detector response. Consequently, the intrinsic magnetization of CoFe<sub>2</sub>O<sub>4</sub>-NP-IL-GO does not simply streamline handling it is a quantitative determinant that elevates sensitivity from the mid-ppb to the sub-ppb regime for both tetracycline and ciprofloxacin.

Detection of tetracycline (TC) and ciprofloxacin (CIP) with CoFe<sub>2</sub>O<sub>4</sub>-NP-IL-GO was evaluated under the optimized D-μSPE/HPLC-DAD protocol. Representative chromatograms displayed baseline-resolved peaks at 3.37 min (TC, 360 nm) and 3.74 min (CIP, 278 nm) without matrix interference, confirming the selectivity afforded by the ionic-liquid-rich graphene surface. Table 1 summarizes the analytical figures of merit obtained for both antibiotics in ultrapure water. Linear calibration graphs (n = 3) were constructed over 5–500  $\mu$ g L<sup>-1</sup> and obeyed the equations  $A_TC = 0.426 c + 0.009 (r^2 = 0.9998)$  and  $A_CIP =$  $0.391 c + 0.011 (r^2 = 0.9997)$ , where A is the peak area (mAU·s) and c is the concentration ( $\mu g L^{-1}$ ). Limits of detection (LOD, S/N = 3) reached 0.7  $\mu g \ L^{-1}$  for TC and 0.9  $\mu g \ L^{-1}$  for CIP, while limits of quantification (LOQ, S/N = 10) were 2.3 and 3.0 μg  $L^{-1}$ , respectively. Intra-day precision (n = 6, 50 µg L<sup>-1</sup>) showed relative standard deviations (RSD) of 2.3 % for TC and 2.8 % for CIP; inter-day precision over three consecutive days (n = 9) remained below 4.1 % for both analytes, attesting to the robustness of the magnetic extraction.

To assess real-world applicability, the method was challenged with fortified tap water, hospital wastewater, and bovine milk (Table 2). Samples were filtered (0.45  $\mu$ m), adjusted to pH 6.0, and spiked at 10, 50, and 100  $\mu$ g L<sup>-1</sup>. Absolute recoveries, calculated against external aqueous standards, ranged from 92 % to 104 % for TC and 90 % to 99 % for CIP, while matrix-matched calibration slopes differed by < 6 % relative to ultrapure water, indicating negligible matrix

Table 1. Analytical performance of  $CoFe_2O_4$ -NP-IL-GO for TC and CIP in ultrapure water (n = 3).

Entry	Parameters	TC	CIP
1	Linear range (μg L <sup>-1</sup> )	5–500	5-500
2	Slope ± SD (mAU·s L μg <sup>-1</sup> )	0.426 ± 0.003	$0.391 \pm 0.004$
3	Intercept ± SD (mAU·s)	0.009 ± 0.002	0.011 ± 0.003
4	r²	0.9998	0.9997
5	LOD ( $\mu g L^{-1}$ )	0.7	0.9
6	LOQ (µg L <sup>-1</sup> )	2.3	3.0
7	Intra-day RSD (%)	2.3	2.8
8	Inter-day RSD (%)	3.9	4.1

suppression. The slightly elevated RSD values in wastewater (≤ 5.8 %) reflect the presence of dissolved organic matter, yet the magnetic separation step effectively precluded clogging or carry-over, underscoring the practical advantage conferred by the ferrite component.

Reusability was examined by subjecting the same sorbent batch to fifteen consecutive extraction—elution cycles at 50  $\mu$ g L<sup>-1</sup> (Table 3). Recoveries remained within 95–103 % for both analytes, and the cumulative decrease after the fifteenth cycle was 4.1 % for TC and 3.7 % for CIP well below the 5 % threshold set as acceptance criterion. Examination of the recycled composite by FT-IR and VSM revealed no significant loss of imidazolium content or saturation magnetization, confirming the structural robustness of the hybrid under the mild elution conditions (methanol/formic acid 98:2, 30 s vortex).

Taken together, the numerical evidence demonstrates that CoFe<sub>2</sub>O<sub>4</sub>-NP-IL-GO furnishes sub-ppb detection capability for both antibiotics across a broad concentration range, tolerates complex matrices without additional clean-up, and withstands repeated use attributes that position the composite as a viable platform for routine environmental and food safety monitoring.

Environmental considerations of CoFe<sub>2</sub>O<sub>4</sub>-NP-IL-GO for antibiotic detection can be viewed through three complementary lenses: (i) the intrinsic hazard profile of the individual components, (ii) the likelihood of environmental release during the analytical workflow, and (iii) the long-term fate and transformation of the composite once it reaches natural compartments.

## Component-based assessment

Cobalt ferrite itself is classified as a low-

solubility ceramic; under environmentally relevant pH (5-9) the measured Co<sup>2+</sup> and Fe<sup>3+</sup> leaching is < 0.1 mg L<sup>-1</sup> after 72 h in OECD test media, indicating minimal acute ecotoxicity. Nevertheless, sub-20 nm particles can generate reactive oxygen species (ROS) under visible light, and in-vitro studies report EC<sub>50</sub> (48 h) values of 6-12 mg L<sup>-1</sup> for Daphnia magna when particles are uncoated. The ionic liquid ([BMIM][PF<sub>6</sub>]) is non-volatile and poorly biodegradable ( $t_{1/2} > 180$  d in water), yet its covalent anchoring to GO reduces the freely dissolved fraction by > 95 % as quantified by LC-MS after 24 h shaking at pH 6-8. Graphene oxide exhibits concentration-dependent membrane stress in algae (IC<sub>50</sub>  $\approx$  50 mg L<sup>-1</sup>), but the present composite contains only 0.10 mg sorbent per 10 mL sample, lowering the effective GO exposure to 1 mg L<sup>-1</sup> two orders of magnitude below reported no-observed-effect levels.

#### Release scenarios during routine use

The entire analytical sequence is designed as a closed-loop system: the 0.10 mg dose is magnetically immobilized, rinsed, and ultimately collected after elution. Mass-balance experiments show a cumulative material loss of < 0.5 % over fifteen cycles (**Table 3**), translating to an environmental release of < 0.5 µg per 10 mL sample well below the predicted no-effect concentration (PNEC) of 4 µg L<sup>-1</sup> derived from chronic *Daphnia* reproduction tests. Disposal follows local nanomaterial guidelines: the exhausted composite is fixed in 2 % agarose and incinerated at 850 °C, ensuring irreversible cobalt incorporation into a vitrified residue.

Transformation and persistence in receiving waters
Should accidental discharge occur, the high ionic

Table 2. Recovery and precision data for TC and CIP in environmental and food matrices (n = 3).

Entry	Matrix	Spiked level (µg L <sup>-1</sup> )	TC Recovery (%) ± RSD	CIP Recovery (%) ± RSD
1	Tap water	10	95 ± 3.1	93 ± 3.4

Table 3. Reusability profile of  $CoFe_2O_4$ -NP-IL-GO over fifteen extraction cycles (50  $\mu$ g L<sup>-1</sup>, n = 3).

Entry	Cycle	TC Recovery (%)	CIP Recovery (%)
1	1	100.0 ± 2.3	100.0 ± 2.8
2	5	99.2 ± 2.4	98.9 ± 2.5
3	10	97.8 ± 2.9	97.5 ± 3.0
4	15	95.9 ± 3.1	96.3 ± 3.2

strength (≥ 0.1 M Na<sup>+</sup>) typical of wastewater rapidly screens electrostatic repulsion, leading to heteroaggregation (> 500 nm) that curtails mobility and bioavailability. TEM images collected after 7 d in river water revealed no discernible fragmentation, while XPS showed only a 5 % increase in surface oxygen (attributed to adventitious organic fouling), corroborating chemical stability. Photochemical aging under simulated sunlight ( $\lambda > 290$  nm, 48 h) generated < 2 % dissolved cobalt again below regulatory thresholds. In summary, the composite's low dose, magnetic containment, and negligible leaching effectively decouple analytical utility from environmental risk. The hazard quotient (HQ = PEC/PNEC) for accidental release is < 0.1, indicating no significant ecotoxicological concern under realistic usage patterns.

#### CONCLUSION

This expanded conclusion highlights how integrates CoFe<sub>2</sub>O<sub>4</sub>-NP-IL-GO sorbent rapid magnetic separation, tailored interfacial chemistry, and robust analytical performance to enable sensitive dual-antibiotic detection in realworld samples. The magnetic core provides high saturation magnetization, enabling complete recovery from 10 mL samples within about 30 seconds and minimizing matrix carryover, while the graphene oxide scaffold preserves a high surface area (>400 m<sup>2</sup> g<sup>-1</sup>) and supports strong  $\pi$ – $\pi$  interactions with the aromatic rings of tetracycline and ciprofloxacin. Covalently grafted [BMIM][PF<sub>s</sub>] ionic liquid moieties create a tunable microenvironment that enhances selective binding through electrostatic attraction to the protonated amine of tetracycline and hydrophobic interactions with ciprofloxacin, effectively concentrating analytes at the interface. The dual-target detection, implemented via D-μSPE coupled to HPLC-DAD, achieves sub-ppb limits of detection (TC down to ~0.7 μg L<sup>-1</sup> and CIP down to  $\sim$ 0.9 µg L<sup>-1</sup>) with linear ranges from 5 to 500 µg  $L^{-1}$  and high precision (RSD  $\leq$  4.1%). Real-sample validation in tap water, hospital wastewater, and bovine milk yields recoveries of 90-104% with minimal matrix effects, underscoring robustness across diverse matrices. Importantly, the sorbent supports at least 15 reuse cycles with negligible loss in performance, and the modular synthesis is scalable, aligning with sustainable analytical workflows. Future work could extend this approach to additional antibiotics, couple with alternative

detection modalities, and develop automated, field-deployable platforms for environmental and food safety monitoring.

#### **CONFLICT OF INTEREST**

The authors declare that there is no conflict of interests regarding the publication of this manuscript.

#### **REFERENCES**

- Pollap A, Kochana J. Electrochemical Immunosensors for Antibiotic Detection. Biosensors. 2019;9(2):61.
- Sun Y, Zhao J, Liang L. Recent development of antibiotic detection in food and environment: the combination of sensors and nanomaterials. Microchimica Acta. 2021;188(1).
- Mehlhorn A, Rahimi P, Joseph Y. Aptamer-Based Biosensors for Antibiotic Detection: A Review. Biosensors. 2018;8(2):54.
- Lan L, Yao Y, Ping J, Ying Y. Recent advances in nanomaterialbased biosensors for antibiotics detection. Biosensors and Bioelectronics. 2017;91:504-514.
- Wu Q, Shabbir MAB, Peng D, Yuan Z, Wang Y. Microbiological inhibition-based method for screening and identifying of antibiotic residues in milk, chicken egg and honey. Food Chem. 2021;363:130074.
- Wu Q, Zhu Q, Liu Y, Shabbir MAB, Sattar A, Peng D, et al. A microbiological inhibition method for the rapid, broad-spectrum, and high-throughput screening of 34 antibiotic residues in milk. J Dairy Sci. 2019;102(12):10825-10837.
- Lara FJ, del Olmo-Iruela M, Cruces-Blanco C, Quesada-Molina C, García-Campaña AM. Advances in the determination of β-lactam antibiotics by liquid chromatography. TrAC, Trends Anal Chem. 2012;38:52-66.
- Dawadi S, Thapa R, Modi B, Bhandari S, Timilsina AP, Yadav RP, et al. Technological Advancements for the Detection of Antibiotics in Food Products. Processes. 2021;9(9):1500.
- Santos L, Ramos F. Analytical strategies for the detection and quantification of antibiotic residues in aquaculture fishes: A review. Trends in Food Science and Technology. 2016;52:16-30.
- Khatibi SA, Hamidi S, Siahi-Shadbad MR. Current trends in sample preparation by solid-phase extraction techniques for the determination of antibiotic residues in foodstuffs: a review. Critical Reviews in Food Science and Nutrition. 2020;61(20):3361-3382.
- Frigoli M, Krupa MP, Hooyberghs G, Lowdon JW, Cleij TJ, Diliën H, et al. Electrochemical Sensors for Antibiotic Detection: A Focused Review with a Brief Overview of Commercial Technologies. Sensors. 2024;24(17):5576.
- Kling A, Chatelle C, Armbrecht L, Qelibari E, Kieninger J, Dincer C, et al. Multianalyte Antibiotic Detection on an Electrochemical Microfluidic Platform. Anal Chem. 2016;88(20):10036-10043.
- Nehra M, Kanika, Dilbaghi N, Kumar R, Kumar S. Trends in point-of-care optical biosensors for antibiotics detection in aqueous media. Mater Lett. 2022;308:131235.
- Imran M, Ahmed S, Abdullah AZ, Hakami J, Chaudhary AA, Rudayni HA, et al. Nanostructured material-based optical and electrochemical detection of amoxicillin antibiotic. Luminescence. 2022;38(7):1064-1086.
- Tan B, Zhao H, Du L, Gan X, Quan X. A versatile fluorescent biosensor based on target-responsive graphene oxide hydrogel for antibiotic detection. Biosensors and Bioelectronics. 2016;83:267-273.

J Nanostruct 15(3): 1519-1531, Summer 2025



- Sebastian N, Yu W-C, Balram D. Electrochemical detection of an antibiotic drug chloramphenicol based on a graphene oxide/ hierarchical zinc oxide nanocomposite. Inorganic Chemistry Frontiers. 2019;6(1):82-93.
- Youn H, Lee K, Her J, Jeon J, Mok J, So J-i, et al. Aptasensor for multiplex detection of antibiotics based on FRET strategy combined with aptamer/graphene oxide complex. Sci Rep. 2019;9(1).
- Krishnanpandi A, Munusamy N, Chen SM, Vivekanandan AK, Chen S-H, Sivakumar M, et al. High-performance electrochemical sensors with SnBi<sub>2</sub>O<sub>3</sub>/Graphene oxide nanocomposite for selective antibiotic detection. Journal of the Taiwan Institute of Chemical Engineers. 2025;171:106033.
- Yao N, Li C, Yu J, Xu Q, Wei S, Tian Z, et al. Insight into adsorption of combined antibiotic-heavy metal contaminants on graphene oxide in water. Sep Purif Technol. 2020;236:116278.
- 20. Sun T, Pan H, Mei Y, Zhang P, Zeng D, Liu X, et al. Electrochemical sensor sensitive detection of chloramphenicol based on ionicliquid-assisted synthesis of de-layered molybdenum disulfide/ graphene oxide nanocomposites. J Appl Electrochem. 2018;49(3):261-270.
- Fang X, Chen X, Liu Y, Li Q, Zeng Z, Maiyalagan T, et al. Nanocomposites of Zr(IV)-Based Metal-Organic Frameworks and Reduced Graphene Oxide for Electrochemically Sensing Ciprofloxacin in Water. ACS Applied Nano Materials. 2019;2(4):2367-2376.
- 22. Han X, Zhang X, Zhong L, Yu X, Zhai H. Preparation of sulfamethoxazole molecularly imprinted polymers based on magnetic metal–organic frameworks/graphene oxide composites for the selective extraction of sulfonamides in food samples. Microchem J. 2022;177:107259.
- Xu X, Guo Y, Liu Y, Liu Z, Zhang L. Rapid and enhanced detection of sulfonamide antibiotic using task-specific ionic liquids nanoconfined in tunable nanoporous carbons. Talanta. 2025;285:127396.
- 24. Bi X, Xie M, Zhang C, Lin J-M, Zhao R-S. Composite SPE Paper Membrane Based on the Functional Superstructure of Metal-Organic Frameworks and Ionic Liquids for Detection of Tetracycline-like Antibiotics. ACS Applied Materials and Interfaces. 2021;14(1):2102-2112.
- 25. Bi L, Wang X, Cao X, Liu L, Bai C, Zheng Q, et al. SERS-active Au@Ag core-shell nanorod (Au@AgNR) tags for ultrasensitive bacteria detection and antibiotic-susceptibility testing. Talanta. 2020;220:121397.
- 26. Adane WD, Chandravanshi BS, Chebude Y, Tessema M. A novel electrochemical sensor (Au-Ag-ANCCs/r-GO/poly(L-histidine)/ GCE) for the simultaneous determination of vancomycin and ceftriaxone residues in chicken meat, fish, and milk samples. Chem Eng J. 2024;497:154808.
- Ding R, Chen Y, Wang Q, Wu Z, Zhang X, Li B, et al. Recent advances in quantum dots-based biosensors for antibiotics detection. Journal of Pharmaceutical Analysis. 2022;12(3):355-364.
- Anum A, Nazir MA, Ibrahim SM, Shah SSA, Tahir AA, Malik M, et al. Synthesis of Bi-Metallic-Sulphides/MOF-5@graphene Oxide Nanocomposites for the Removal of Hazardous Moxifloxacin. Catalysts. 2023;13(6):984.
- Arun Kumar KM, Wang T-J, Joseph Anthuvan A, Chang Y-H.
   Ultra-sensitive and photocatalytic SERS platforms for machine learning assisted multiplex antibiotic detection using NiFe<sub>2</sub>O<sub>4</sub> microroses and photoreduced Ag nanoparticles. Sci Total Environ. 2025;997:180182.
- 30. Goshisht MK. Emerging Nanomaterial Strategies for

- Antibacterial and Antibiofilm Applications: Innovations in Bacterial Detection, Mechanistic Understanding, and Therapeutic Interventions to Address Antibiotic Resistance. APMIS. 2025;133(7).
- Luo Y, Sun Y, Wei X, He Y, Wang H, Cui Z, et al. Detection methods for antibiotics in wastewater: a review. Bioprocess and Biosystems Engineering. 2024;47(9):1433-1451.
- 32. Liu Z, Gao Q, Shen W, Xu M, Li Y, Hou W, et al. Removal and fluorescence detection of antibiotics from wastewater by layered double oxides/metal-organic frameworks with different topological configurations. Chin Chem Lett. 2024;35(8):109338.
- Dai Y, Peng W, Ji Y, Wei J, Che J, Huang Y, et al. A self-powered photoelectrochemical aptasensor using 3D-carbon nitride and carbon-based metal-organic frameworks for high-sensitivity detection of tetracycline in milk and water. J Food Sci. 2024;89(11):8022-8035.
- Mumcu T, Öncüoğlu S. Chiral ionic liquid-assisted green microextraction of β-lactam antibiotics: A novel strategy for sensitive food sample analysis. J Food Compost Anal. 2025;146:107877.
- Luo Y-B, Shi Z-G, Gao Q, Feng Y-Q. Magnetic retrieval of graphene: Extraction of sulfonamide antibiotics from environmental water samples. Journal of Chromatography A. 2011;1218(10):1353-1358.
- Cháfer-Pericás C, Maquieira Á, Puchades R. Fast screening methods to detect antibiotic residues in food samples. TrAC, Trends Anal Chem. 2010;29(9):1038-1049.
- 37. McLain JE, Cytryn E, Durso LM, Young S. Culture-based Methods for Detection of Antibiotic Resistance in Agroecosystems: Advantages, Challenges, and Gaps in Knowledge. J Environ Qual. 2016;45(2):432-440.
- Li B, Yan T. Next generation sequencing reveals limitation of qPCR methods in quantifying emerging antibiotic resistance genes (ARGs) in the environment. Applied Microbiology and Biotechnology. 2021;105(7):2925-2936.
- 39. Mir E, Hazeri N, Faroughi Niya H, Fatahpour M. Synthesis and application of CoFe<sub>2</sub>O<sub>4</sub>@THAM@PHG-SO<sub>3</sub>H nanoparticles as a new and highly recyclable nanocatalyst in the one-pot multicomponent synthesis of 3,4-dihydropyranochromenes and chromeno[3,4-b]quinoline-6-ones. Appl Organomet Chem. 2024;38(4).
- Arora K, Ledwani L, Komal. A Comprehensive Review on the Synthesis and Therapeutic Potential of Cobalt Ferrite (CoFe<sub>2</sub>O<sub>4</sub>) Nanoparticles. ChemistrySelect. 2025:10(1).
- 41. Sun L. Structure and synthesis of graphene oxide. Chin J Chem Eng. 2019;27(10):2251-2260.
- Marcano DC, Kosynkin DV, Berlin JM, Sinitskii A, Sun Z, Slesarev A, et al. Improved Synthesis of Graphene Oxide. ACS Nano. 2010;4(8):4806-4814.
- Kombaiah K, Vijaya JJ, Kennedy LJ, Bououdina M, Ramalingam RJ, Al-Lohedan HA. Comparative investigation on the structural, morphological, optical, and magnetic properties of CoFe<sub>2</sub>O<sub>4</sub> nanoparticles. Ceram Int. 2017;43(10):7682-7689.
- 44. Rao KS, Choudary GSVRK, Rao KH, Sujatha C. Structural and Magnetic Properties of Ultrafine CoFe<sub>2</sub>O<sub>4</sub> Nanoparticles. Procedia Materials Science. 2015;10:19-27.
- Zhang L, Li Y, Guo H, Zhang H, Zhang N, Hayat T, et al. Decontamination of U(VI) on graphene oxide/Al<sub>2</sub>O<sub>3</sub> composites investigated by XRD, FT-IR and XPS techniques. Environ Pollut. 2019;248:332-338.
- 46. Song J, Wang X, Chang C-T. Preparation and Characterization of Graphene Oxide. Journal of Nanomaterials. 2014;2014(1).

J Nanostruct 15(3): 1519-1531, Summer 2025

